Re-entrant Appearance of Phases in a Relaxed Langmuir Monolayer of Tetracosanoic Acid as Determined by X-Ray Scattering

Re-entrant appearance of phases in a relaxed Langmuir monolayer of tetracosanoic acid as determined by x-ray scattering

D. K. Schwartz,[a] M. L. Schlossman,[b] and P. S. Pershan
Department of Physics and Division of Applied Sciences, Harvard University, Cambridge, Massachusetts 02138

(Received 22 July 1991; accepted 22 October 1991)

The structure of the fully relaxed phases of a Langmuir monolayer of tetracosanoic acid is determined by x-ray diffraction and reflection along an isotherm at ~20.5 °C. Isotherms taken by allowing the surface pressure to stabilize between incremental compressions are seen to be qualitatively different from the constant-rate nonrelaxed isotherms typically seen in the literature. At low densities the monolayer consists of an inhomogeneous film of islands of a crystalline (or hexatic) phase with molecular tilt ordering that is analogous to that of the smectic *I* liquid crystal. Small amounts of impurities (~0.5% of the monolayer) account for the change in surface pressure with area in this region. Upon compression to the point that the free space between islands becomes negligible the film appears homogeneous. On further compression the time required for full relaxation becomes long (i.e., ~ hours), the tilt angle of the molecular axis decreases and the x-ray unit cell is compressed. Including this homogeneous *I* phase the phase sequence observed by diffraction upon compression is *I-U-I-U*, where *U* refers to an untilted orthorhombic phase. The outer two phases of this sequence are pure phases which form homogeneous monolayers, but the inner two are inhomogeneous phases each coexisting with an amorphous phase that does not have an observable diffraction signal. At the boundaries demarcating the *I* and *U* phases, a phase whose tilt ordering is analogous to that of a smectic *F* phase is seen to coexist. The preceding phase sequence is sensitive to the degree of relaxation permitted the monolayer after an incremental compression. In particular, if the monolayer is not allowed to relax completely after each compression, the untilted *U* phase may never appear. The $U \leftrightarrow I$ transition is shown to be reversible for a relaxed monolayer.

I. INTRODUCTION

Throughout the long history of thermodynamic studies of Langmuir monolayers (LM) of long chain carboxylic acids the issue of relaxation and equilibration has been occasionally though infrequently addressed. It is widely recognized that upon compression the monolayer requires time (seconds to hours) for the surface pressure to relax to a steady-state value,[1-3] nevertheless, most published isotherms are measured at a constant rate of compression which often does not allow sufficient time for relaxation. The physical significance of the phase diagrams which are extracted from isotherms in which the monolayer is not fully relaxed is ambiguous, particularly if the observed phases depend on the rate of compression. The recent application of surface-sensitive x-ray scattering techniques to the investigation of the structures of monolayer phases allows for direct observation of the intermolecular structure of phases identified from pressure-area (π-A) isotherms. One study by Lin *et al.* indicated that, for a certain temperature range, after a "one-stroke" (continuous) compression from approximately 0 dyn/cm to the desired pressure (15, 20, or 25 dyn/cm) a pseudohexagonal phase will relax to a hexagonal phase.[4] Unfortunately, except for that study and a previous short report of the present study[5] the issue of equilibration has not been addressed in any other x-ray scattering study. X-ray scattering data has typically been taken while the LM was either still in the process of relaxing,[6] or while continually adjusting the area of the LM in order to keep the surface pressure relatively constant.[7,8] In addition, diffraction data has often been reported[9,10,7] at pressures exceeding those for which the LM is stable in the limit of either slow compression rates,[2,11] or—as we will show below—when allowed to relax completely.

We will demonstrate in this manuscript that when the LM of tetracosanoic acid ($CH_3(CH_3)_{22}COOH$, referred to in this manuscript as C24), at pH 2 and ~20.5 °C, is allowed to relax completely following each incremental compression, both the isotherm and the x-ray scattering results are different from those that are obtained when the film is not allowed to equilibrate. For some portions of the π-A isotherm, following an incremental compression the time constant of the observed exponential decay of π to its equilibrium value is of the order of 1 or 2 h. Full relaxation may require 5 or 6 h during which dramatic structural changes may occur for very small changes (~0.01 to 0.1 dyn/cm) in surface pressure. Since C24 isotherms measured at a constant rate of compression can have a qualitatively different shape than similar ones taken under equilibrium conditions at the same temperature, it is essential to understand the nature of the relaxation process that we report and to then ask what it is that phase diagrams reported on the basis of

[a] Present Address: Department of Chemical and Nuclear Engineering, University of California, Santa Barbara, Santa Barbara, CA 93101.
[b] Present Address: James Franck Institute, Consortium for Advanced Radiation Sources, The University of Chicago, Chicago, Illinois 60637.

 0021-9606/92/032356-15$06.00

these two different types of isotherms tell us about the basic, equilibrium nature of the LM.

II. TROUGH DETAILS

All experiments were performed with a custom Langmuir trough that was mounted inside of a sealed aluminum box (22 in. $\times$ 7 in. $\times$ 7 $\frac{7}{8}$ in.).[12] The box was designed such that it was possible to add or extract water, aspirate the surface, change monolayer density, and measure the surface pressure and temperature without opening the box and disturbing the clean experimental environment of prepurified nitrogen. The box was temperature controlled to within 0.1 °C and included both x-ray windows—appropriate for either specular reflectivity or surface diffraction measurements—and an optical window to allow visual inspection of the liquid surface. Monolayer surface density was controlled, and temperature and surface tension were measured remotely by computer.

The trough was milled from a solid piece of teflon that was rigidly attached to a piece of OFHC copper. A solid teflon barrier placed across the top edge of the trough to confine the Langmuir film to a specified area could be moved under computer control to vary the density of the film. The total area of the monolayer was typically varied from a maximum of ~ 200 to ~ 50 cm^2 and the water was approximately 7.0 mm deep. In order to minimize effects of low frequency mechanically induced surface vibrations the depth of the water in the part of the trough that was probed by x rays was kept to ~ 0.2–0.3 mm by placing an ~ 6.7 mm thick quartz flat (~ 100 mm $\times$ 12.5 mm) beneath the illuminated area.

The surface tension, γ_{surface}, and hence surface pressure, $\pi = \gamma_{\text{water}} - \gamma_{\text{surface}}$, was measured using a Wilhelmy plate balance consisting of a leaf spring, a displacement transducer (LVDT), and a plate made of filter paper with a pore size of 0.22 μm.[13] Water wet the filter paper with a contact angle of 0° so that the force exerted on the paper when inserted vertically into the water was simply the surface tension times twice the length of the plate. This force deflected the leaf spring and the deflection was measured by the LVDT. The balance was calibrated using known weights to determine the overall proportionality constant and to insure that all measurements were in a linear regime of the spring and transducer. The surface tension was measured *in situ* with a resolution of 0.01 dyn/cm and an accuracy of ± 0.5 dyn/cm. The large error in the accuracy is due to variations in water level from monolayer to monolayer; however, due to the high humidity in the sealed aluminum box the water level for an individual monolayer did not change so long as the box was not opened. Variations in the water level on the order of μm were easily detectable by the x rays. The density of a deposited monolayer was varied by moving the barrier along the trough under computer control. The homemade translation stage was designed to run without lubrication and with negligible backlash (0.001 in.). The stage was driven by a dc motor with an optical rotary encoder to measure position.

The water for the experiments was obtained from a Millipore[13] Milli-Q UV + system fed by a Milli-RO system. The pH of the water was adjusted to 2.0 ± 0.1 by adding pure HCl (Ref. 14) and placed in an air-filtered 4 l pyrex bottle. The pH of the subphase produced this way was observed to change by less than 0.05 when sitting in either the bottle or the trough for periods of the order of 1 week. Typically the water for the subphase was withdrawn from the bottom of the bottle after a few hours. We believe that this allowed sufficient time for some of the remaining surfactant contaminants to rise to the water surface, and in this way the bottle storage probably provided some additional purification. A closed system of teflon TFE plumbing was used to transfer the water from the bottle to the trough. A Pasteur pipette attached to a clean mechanical pump was used both to remove liquid from the trough and to aspirate the surface to clean it of residual contaminants. The pipette was attached to a teflon bellows which allowed it to be moved around inside the box while still keeping the box airtight. Tetracosanoic acid obtained from either Fluka[15] or Sigma[16] was used without further purification and gave similar results. Baker Resi-Analyzed chloroform[17] was used as a solvent. In place of pure chloroform as a solvent, chloroform/benzene mixtures were also tried and found to give identical results.

The temperature of the system was controlled by two Neslab closed cycle systems to about 0.1 °C. One controller sent temperature controlled liquid (90% water/10% ethylene glycol) through a gold plated copper plate directly beneath the trough. The other controller sent liquid through an upper cooling plate suspended about 1 in. above the water surface and through copper tubing in thermal contact with the outside surfaces of the walls and roof of the aluminum box. The box was covered with closed-cell foam insulation. Temperature was measured with thermistors on the plate below the trough, on a second gold plated copper plate that was thermally floating halfway between the water surface and the upper cooling plate, on the upper cooling plate, and on the roof of the box. In order to minimize convection and keep the x-ray windows free of condensation the controllers were set so that the plate below the trough was 2–3 °C colder than the upper cooling plate. The box was mounted on a delrin spacer (for temperature isolation) and then on a kinematic mount tilt stage.

The use of consistent cleaning procedures was found to be very important in achieving a clean environment for the trough studies. Before use the apparatus was disassembled, cleaned, and reassembled in a clean hood. The trough was repeatedly flushed with water by filling it and then removing the water with the built-in aspirator pipette. Typically this was done 20–50 times over a period of 2 or 3 days before the system was clean enough to take isotherms. To prepare a clean water surface we filled the trough quite high and allowed the surface pressure to equilibrate. We then moved the barrier to the end of the trough near the aspirator, concentrating any residual insoluble impurities and vacuumed the surface with the pipette to remove these impurities. At this stage, the enclosure was refilled with nitrogen and allowed to equilibrate again. In order to test the cleanliness of the surface, the barrier was moved across the trough, thus reducing the surface area available to impurities by a factor of 3 or 4. If the surface tension changed by less than 0.05 dyn/cm, and

remained stable for a minimum period of a $\frac{1}{2}$ h, we considered the surface to be clean enough to use. Usually the changes observed on compression were about 0.02 dyn/cm as shown in Fig. 5(b). Similar tests were also performed following deposition of the pure solvent on the water surface. Following deposition it took approximately 15 min for the pressure to stabilize. This is probably due to some combination of evaporation of the solvent and the time necessary for the initial humidity in the box to be restored; however, once the surface tension had stabilized the surface tension changes following compression were indistinguishable from those observed for the bare water surface.

In order to deposit a film without introducing contaminants we used a graduated glass microliter syringe with a teflon tipped plunger[18] and a 12 in. needle. While flowing clean nitrogen gas into the enclosure a small (3/4 in. diam) port was opened on the enclosure wall and the needle inserted. The solution was added to the water surface drop by drop by carefully touching the drop hanging from the end of the needle to the water surface without submerging the needle tip. The port was then closed and the overpressure of clean nitrogen in the enclosure was stabilized at ~ 1 psi. The relaxation of surface pressure was continuously monitored for periods of the order of 15 min until it became stable. Errors introduced by the reading of the graduated syringe and differences in water level (which cause variations in the area of the exposed liquid) resulted in approximately 2%–4% errors in area/molecule from one film to another.

III. SPECTROMETER DETAILS

The x-ray measurements were made at beam line X22B of the National Synchrotron Light Source at Brookhaven National Laboratory. The data reported here are the result of more than 2.5 months of beamtime over the period of a year and represent detailed studies of approximately 30 monolayers. The liquid surface spectrometer has been described in detail elsewhere,[19,20] but the general design is as follows (see Fig. 1): the x rays are focused by a doubly curved mirror which is about 14 m from the x-ray source and about 6 m upstream of the hutch. The x rays are monochromated by a single bounce Ge(111) crystal which is located just outside of the entrance of the hutch. A slit $S1$, after the first monochromator, is closed down just enough to slightly trim the beam. A second Ge(111) crystal, 2 m after the first, reflects the beam down to the desired angle α with respect to the surface. A slit $S2$ before the sample position fixes the size of the beam hitting the sample. Typical $S2$ slit settings were a vertical size of $h_2 = 0.1$ mm and a horizontal size $w_2 = 2$ mm. The focused beam at the sample has an angular divergence determined by the x-ray source, the optics, and the slits and is given by $\Delta\alpha \approx 6\times 10^{-5}$ rad in the vertical and $\Delta\Phi \approx 2\times 10^{-3}$ rad in the horizontal. The distances from crystal to sample and from sample to detector were both about 600 mm. The x-ray intensity incident upon the sample was monitored by a scintillation detector, placed after $S2$ and immediately before the sample, which recorded x rays scattered perpendicular to the main beam. Another slit $S3$ is placed after the sample, primarily to reduce background scattering. For diffraction measurements Soller slits, with

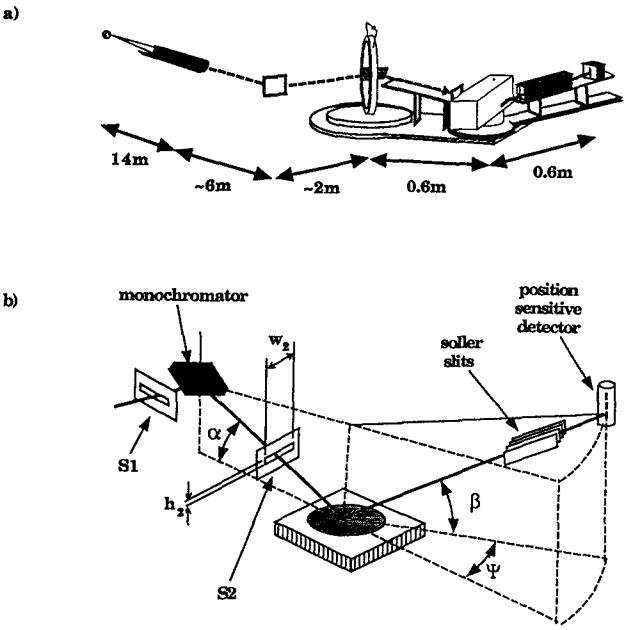

FIG. 1. (a) Schematic illustration of beam line X22B at the National Synchrotron Light Source (NSLS). (b) Schematic illustration of the liquid surface spectrometer that was used for the present experiments.

the leaves oriented vertically, were placed just before the detector. The horizontal angular spread accepted by the Soller slits was $\Delta\Psi \approx 3\times 10^{-3}$ rad. A Braun quartz wire position-sensitive detector placed behind the Soller slits, with the wire mounted vertically, enabled measurements to be simultaneously recorded over a range of angles β, with respect to the surface. For each detected x ray a count was added to one of the 1024 channels into which the 50 mm length of the wire was electronically partitioned. This resulted in a maximum resolution of $\Delta\beta \approx 8\times 10^{-5}$ rad. The physics for the present measurements made this fine resolution unnecessary and the channels were combined into 4 bins, of 256 channels each, giving a resolution of approximately 0.02 rad or $\Delta Q_z \cong 0.06$ Å^{-1}. The detector arm could be rotated about a vertical axis through the sample position (varying Ψ) and moved vertically (varying β) to access a wide range of scattered wave vectors.

The wave vector transferred, $\mathbf{Q} = \mathbf{k}_{\text{out}} - \mathbf{k}_{\text{in}}$, is related to the spectrometer angles by the following equations:

$$Q_x = (2\pi/\lambda)\cos\beta \sin\Psi,$$

$$Q_y = (2\pi/\lambda)\,[\cos\beta\cos\Psi - \cos\alpha],$$

$$Q_z = (2\pi/\lambda)\,[\sin\alpha + \sin\beta\,];$$

however, for a two dimensional powder the only physically significant quantities are Q_z and the amplitude of the in-plane wave vector

$$Q_\perp = \frac{2\pi}{\lambda}\,[\cos^2\alpha + \cos^2\beta - 2\cos\alpha\cos\beta\cos\Psi]^{1/2}.$$

With a wavelength $\lambda = 1.527 \pm 0.006$ Å, and $\alpha = 0.14°$ (slightly less than the critical angle for total external reflection 0.15°) the spectrometer can access approximately $-2 \leqslant Q_\perp \leqslant 2$ Å^{-1} and $0 \leqslant Q_z \leqslant 1$ Å^{-1}.

IV. ISOTHERMS

Two fundamentally different types of isotherms were taken, under computer control, over a temperature range from 18–25 °C. What we believe to be near equilibrium isotherms (Type I) were taken by making a sequence of small area compressions separated by variable waiting periods. During the waiting periods, pressure measurements were automatically recorded at equal time intervals of between 1.5 and 2 min. The waiting periods were automatically terminated, and the next compression step was taken only after five successive measurements were equal to one another within 0.01 dyn/cm. Complete isotherms taken in this manner took as long as 2 or 3 days. This placed very stringent conditions on the stability and the cleanliness of the entire system. In addition, it was absolutely essential that the material chosen for these experiments have negligible solubility in the subphase. Figure 2(a) shows all of the readings taken versus time for one complete isotherm at 20.0 °C.

Isotherms in which the surface pressure was not necessarily stabilized were taken in a similar manner, except that the waiting time between incremental compressions was set at some predetermined fixed value. For this type of isotherm (Type II) a data point was typically taken every 0.2 Å^2/molecule with a waiting time of 60 s between compressions. Thus an entire Type II isotherm took 1 to 2 h to measure. This method, as well as the method of continuous compression, is routinely used by many experimenters;[21,22] however, as can be seen in Fig. 3 the Type II isotherms obtained in this way differ in several respects from the Type I isotherms. For example, the pressures in Type II isotherms are generally higher at the same area and temperature. This is demonstrated in Fig. 3(b) for isotherms at 22.0 °C. Also, the Type II isotherms continue to a much higher pressure before collapse (often as high as 40–50 dyn/cm), while the maximum attainable surface pressures for the Type I isotherms are in the range 11–15 dyn/cm as demonstrated in Fig. 4.

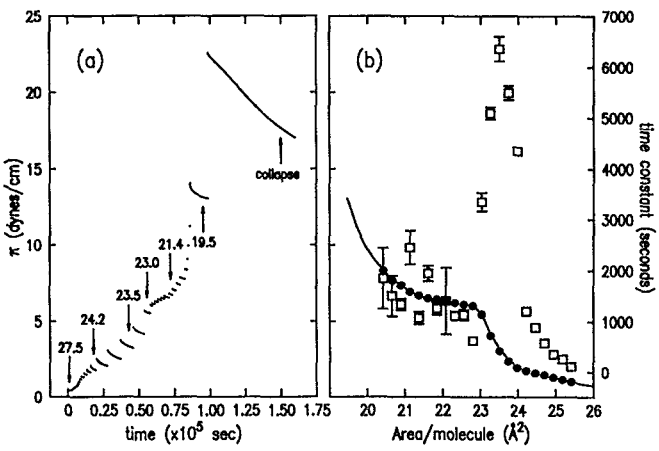

FIG. 2. (a) Pressure readings vs time for an entire isotherm at 20.0 °C. Each jump corresponds to an incremental compression after which the monolayer is allowed to relax. A few values of area/molecule are given as a guide (with arrows pointing to the associated region of the plot). (b) The isotherm (line) corresponding to the data in (a) along with the relaxation times τ (open squares) and the final values of the relaxation fits π_∞ (solid circles) as described in Eq. (2).

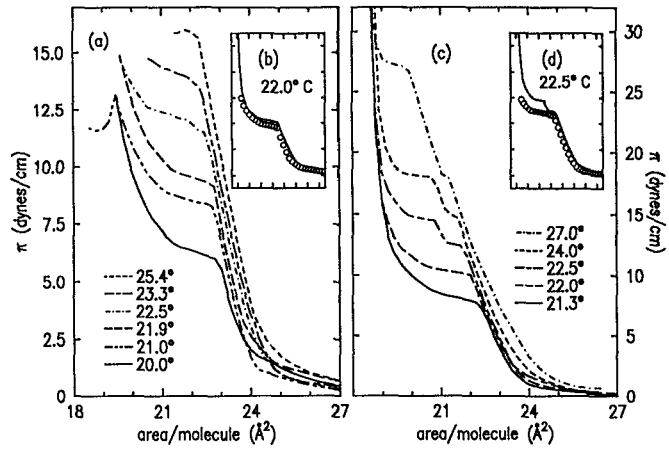

FIG. 3. (a) Type I, or fully relaxed isotherms for a range of temperatures. Data beyond the collapse pressure is shown for one temperature (21.0 °C). (b) A direct comparison between a type I (open circles) and type II (solid line), or nonrelaxed isotherm at 22.0 °C where the shapes are the same and π for the type II isotherm is only slightly larger. (c) Type II, or nonequilibrium isotherms over a range of temperatures. (d) Comparison between the two types of isotherms at 22.5 °C where the shapes are distinctly different. The open circles and the line have the same meaning as in (b).

The collapse of a Type I isotherm is illustrated for one temperature (21.0 °C) in Fig. 3(a). Most importantly, the qualitative shapes of the two types of isotherms are often different at the same temperature. For example, at 22.5 °C and above, the Type II isotherms have two kinks, which would generally be interpreted as two phase transitions.[22] In particular, this sequence of Type II isotherms in Fig. 3(c) is reminiscent of isotherms near a triple point. However, when the surface pressure is allowed to stabilize, the Type I isotherms do not exhibit a triple point at these temperatures. The Type I isotherms at these temperatures have only one kink. Figure 3(d) shows a direct comparison between these two types of isotherms at 22.5 °C.

We will present grazing incidence diffraction results on the monolayers which, along with similar results by others,[8,10,23] indicate one type of two-dimensional crystalline or

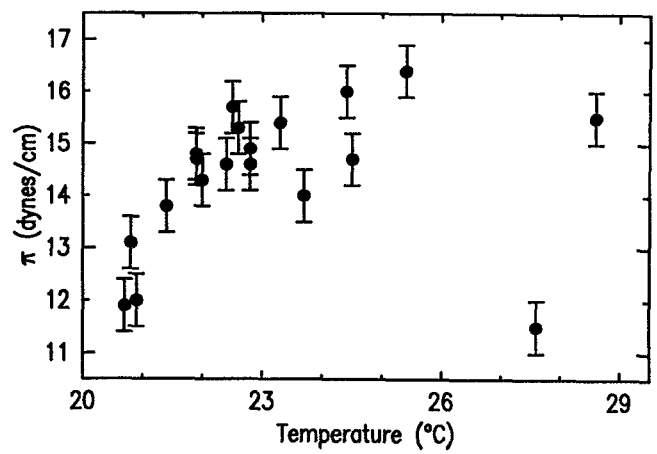

FIG. 4. Collapse pressures for equilibrium isotherms as a function of temperature.

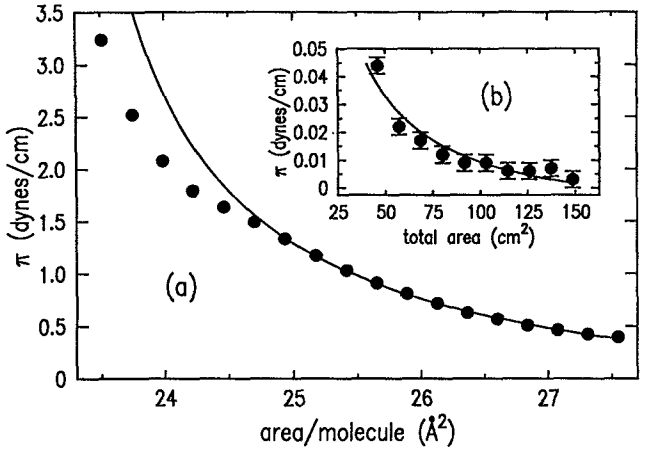

FIG. 5. (a) Large area portion of isotherm with fit to excluded-area ideal gas law. The solid line is the best fit to Eq. (1) when only the data with $A_M \geqslant 24.9$ Å^2 are included in the fit; $A_0 = 22.8 \pm 0.14$ Å^2, $c = 0.009 \pm 0.001$, $\pi_0 \cong -0.5$ dyn/cm, and chi-squared = 6.6. (b) A typical compression isotherm for a clean water surface.

hexatic phase for $A \geqslant 21.5$ Å^2. For $A \geqslant 23$ Å^2 the x-ray diffraction pattern is independent of A. This fact, by itself would normally suggest coexistence between the crystalline or hexatic phase and a disordered phase. However, for a pure system π should not change during compression of a macroscopic area containing two thermodynamically coexisting phases. As can be seen in Fig. 5(a), for $A \geqslant 25$ Å^2, there is a slow rise in pressure with decreasing area. If we assume that impurities fill the space between the crystallites and behave as a two-dimensional ideal gas, then the pressure should satisfy

$$\pi - \pi_0 = ck_B T/(A - A_0), \tag{1}$$

where c is the ratio of the number of impurities to the number, N, of monolayer molecules in the film, A_0 is the area/molecule filled by the crystalline domains, and π_0 ($\cong -0.5$ dyn/cm) accounts for systematic errors in the absolute value of π. The solid line in Fig. 5(a) representing this functional form, describes the isotherm quite well at large areas with $c = 0.009 \pm 0.001$ and $A_0 = 22.8 \pm 0.14$ Å^2. As data points at smaller areas are included in the range fit, the value of chi squared is constant at first (smallest values of chi squared ~ 2) but then rises precipitously to values ~ 60. The best values for the adjustable parameters, c and A_0, were taken from the fit at the smallest area before the rise in chi squared. Typical best fit values of c ranged between 0.005 and 0.01 implying that impurities were on the order of 0.5%–1% of the number of molecules deposited in the monolayer. Although this is between 5 and 10 times larger than the number of impurities that were on the clean surface it is still a reasonable number, suggesting that the largest fraction of impurities were deposited along with the monolayer.

When the film was in the large area region (i.e., $A \geqslant 25$ Å^2) the surface pressure stabilized quickly, on the order of 30 s after a compression. This is understandable if the crystalline, or hexatic, domains were mostly separated. However, at some point around 25 Å^2/molecule the decay time rises dramatically and we suspect that this indicates the onset of a region in which the crystalline domains are being pressed together; e.g., at this point the pressure can only relax through annealing of defects in the long range crystalline, or hexatic, order of the domains. In order to get a quantitative measure of the relaxation rate the time dependence of the pressure, following each incremental compression, was fit to the form

$$\pi = Ae^{(t - t_0)/\tau} + \pi_\infty . \tag{2}$$

Figure 2(b) shows the typical results of such fits at 20.0 °C for the relaxation times τ and the limiting pressures π_∞. As can be seen the values π_∞ match the measured isotherm very well. This vindicates the relaxation procedure we use to measure the isotherms and, similarly, to prepare the monolayers for x-ray measurements. With decreasing area the relaxation times rise, as expected, around 25 Å^2, but they decrease relatively abruptly following the decrease in $d\pi/dA$ as the monolayer enters the "plateau region." At higher pressures the relaxation times often appear to rise again. However, in this region the exponential form is no longer as good a description of the relaxation process.

We believe that the long equilibration times that precede the kink are due to the relaxing of grain boundaries between domains that are brought together. Clearly, if this relaxation is not allowed to occur (say by fast compression), the internal pressure within the crystalline domains should be different from the macroscopically measured surface pressure, which would not necesarily be an acceptable intrinsic thermodynamic variable.

The relaxation procedure outlined above was also used to prepare the monolayers for x-ray measurements. The additional time required for the diffraction measurements, including the repetitions required to ensure the stability of the peaks, resulted in surface pressure relaxation rates that were no larger than approximately 0.01 dyn/cm-h. Most of the monolayers studied with x-ray scattering were spread at $\pi \leqslant 3$ dyn/cm and then compressed in steps of 0.1 or 0.2 Å^2; however, to study lower densities a few monolayers were spread at lower π. No monolayers were used for more than 3 days. When π stabilized the diffraction patterns were also stable, and successive steps in area A were not taken until both were stable. There was no evidence of longer term drifts that might have been induced by x-ray damage to the sample.[10,4]

V. X-RAY BACKGROUND

A. Reflectivity

X-ray specular reflectivity has been used successfully to obtain quite detailed information about the electron density profile near the surfaces of both simple and ordered liquids[24–26,20,27–34] as well as of crystalline and amorphous solids.[35–44] The geometry for reflectivity is the same as that shown in Fig. 1(b); however, since specular reflection is only observed when $\alpha = \beta$ and $\Psi = 0$, the data can be regarded as a function of $Q_z = (4\pi/\lambda)\sin\alpha$ with $Q_x = Q_y = 0$. This implies that the theoretical form of the

differential cross section for specular reflectivity from a perfectly flat surface can be expressed as the product of a function of Q_z and delta functions in Q_x and Q_y. In view of the fact that diffuse scattering from the bulk liquid (and air, etc.) will generally be a slowly varying function of both Q_x and Q_y it is straightforward to remove the contribution that background scattering makes to the total signal observed when the reflectometer is in the specular position by simply subtracting the intensity detected when the spectrometer is tuned slightly away from the specular at a small but finite Q_y. On the other hand, for liquid surfaces, the theoretical form for diffuse scattering from thermally excited capillary waves varies as $1/(Q_x^2 + Q_y^2)$ and the separation of specular reflectivity from surface diffuse scattering is more subtle.[24,25,45,46]

A convenient way to analyze reflectivity from surfaces is to compare it to the reflectivity expected from an ideal "step-function" interface, i.e., the Fresnel equation. Because the dielectric constant at x-ray frequencies is typically less than that in vacuum there is a critical angle below which there is total external reflection. Beyond that angle the reflectivity is given by

$$R_F = \left(\frac{Q_z - \sqrt{Q_z^2 - Q_c^2}}{Q_z + \sqrt{Q_z^2 - Q_c^2}}\right)^2.$$

The critical wave vector Q_c is given by

$$Q_c^2 = \frac{16\pi\rho e^2}{mc^2},$$

where ρ is the electron density. This expression for R_F is the exact solution for reflection of TE polarization (appropriate for this geometry at the synchrotron) from the ideal "step-function" interface; however, at the small angles used in this experiment the polarization correction is negligible and this form can be used for either polarization. When $Q_z \gg Q_c$, $R_F(Q_z)$ is small compared to unity, therefore, the reflectivity, $R(Q_z)$, from a more realistic density profile, can be calculated in the kinematic approximation

$$\frac{R(Q_z)}{R_F(Q_z)} \approx \left|\frac{1}{\rho_\infty}\int_{-\infty}^{\infty} e^{iQ_z z}\frac{d\langle\rho(z)\rangle}{dz}\,dz\right|^2, \tag{3}$$

where ρ_∞ refers to the electron density in the bulk material (water) and $\langle\rho(z)\rangle$ is the electron density at some height z averaged over appropriate length scales in the x and y directions.

Reflectivity data is typically analyzed by postulating a parameterized model for the electron density of a given system and fitting the model to the data using Eq. (3). In view of the fact that there is no way to establish the uniqueness of the model that fits the data, in the absence of some theoretical basis for the model, the final interpretation of the results must rely on physical intuition regarding what constitutes a reasonable model. Furthermore, since the appropriate length scale over which $\langle\rho(z)\rangle$ is averaged varies from a thousand Angstroms up to one or more microns it is important to distinguish between values of $\langle\rho(z)\rangle$ that reflect the local electron density of a homogeneous interface and the average values of inhomogeneous interfaces. Since it is now clear from many experiments on quite diverse systems that LM are macroscopically inhomogeneous in large parts of their pressure/area phase diagrams[47-50] it is important to recognize that it is only in those regions where the LM are homogeneous that the present approach to interpretation of x-ray specular reflectivity can be simply used to determine microscopic features of the LM.

For the present system of a Langmuir monolayer of C24 on water the model was constructed as follows. Assuming a uniform LM on water and progressing downwards from the vapor the basic features of a model for the electron density profile are the following:

(1) the width of the interfacial region between vapor and alkane tails,

(2) the amplitude of the electron density in the tail region,

(3) the additional electron density in the area of the head group,

(4) the distance between the alkane-vapor interface and the position of the head group,

(5) the width of the head group.

This requires a minimum of five free parameters. However, there are other additional details of the monolayer profile that need to be specified. For example, this model must include some specific functional form for both the tail/vapor interface and the electron density at the head group position. In addition it is possible that there is some fine structure along z in the electron density of the tail region, etc. In principal these types of details can be obtained from a sufficiently well ordered surface. However, as will be seen below, these details can not be resolved in the present study, because our reflectivity data could only be measured to $Q_z \leqslant 0.6$ Å^{-1}, making fits fairly insensitive to structural details on length scales $\ll(\pi/0.6)(\simeq 5$ Å$)$. Therefore, the sensible thing to do is to choose a simple model that determines the features in which we are interested, keeping in mind that the quality of the fit may not be as good as with a more complicated parameterization that would probably be neither unique nor insightful.

One such model for a monolayer density is the following:

$$\frac{\rho(z)}{\rho_\infty} = \frac{A_1}{2}\left[1 + \operatorname{erf}\left(\frac{z}{\sqrt{2}\sigma_1}\right)\right] + \frac{A_2}{\sqrt{2\pi}\sigma_2}e^{-(z-L)^2/2\sigma_2^2} + \frac{(1-A_1)}{2} \times\left[1 + \operatorname{erf}\left(\frac{z-L}{\sqrt{2}\sigma_3}\right)\right], \tag{4}$$

where $\operatorname{erf}(x)$ is the standard error function. Each parameter above can be identified with one of the features mentioned earlier. The width of the tail/vapor interface is given by σ_1, while A_1 specifies the electron density in the tail group region (normalized to the density of water). The parameter L specifies the distance from the tail/vapor interface to the head group. The integrated electron density in the head group is given by A_2, and the width of the head group region is given by σ_2. The parameter σ_3 is coupled to σ_2 and adds little physical insight. Since the data is not very sensitive to the precise value of σ_3 as long as it is reasonably close to that

of σ_2, we simply fix σ_3 at a value of 3 Å and do not allow it to vary in the fitting procedure.

B. Diffraction

The use of grazing incidence diffraction (GID) to study surface structure has been widely applied to solid surfaces.[51–58,39] The GID technique became feasible as a result of the development of synchrotron x-ray sources, i.e., because such sources have very high intensity per solid angle and per band width, diffraction signals from single monolayers can have count rates of the order of 10–100 counts/s. Since stray scattering from other sources can be reduced to comparable levels these rates are adequate for detailed diffraction studies. The GID technique essentially eliminates diffuse scattering from the bulk material below the surface by restricting the incident angle α (see Fig. 1) to be smaller than the critical angle, $\phi_c = Q_c\lambda/4\pi$, for total external reflection. Under this condition the incident wave only penetrates into the bulk evanescently with an exponential characteristic length $\sim\lambda/4\pi\sqrt{\phi_c^2 - \phi^2}$ which is of the order of 50 Å when $\phi \ll \phi_c$. The fact that diffuse scattering from this thin layer is not significantly larger than Bragg scattering from a single monolayer is what renders the GID technique practical.

The kinematics of GID scattering from LM can be discussed in terms of diffraction from two dimensional crystals. An arbitrary two-dimensional Bravais lattice can be described by three parameters, e.g., two basis vector lengths, a_1 and a_2, and the angle between them, γ, as shown in Fig. 6. If the lattice vectors are written as

$$\mathbf{a}_1 = \begin{pmatrix} a_1 \\ 0 \end{pmatrix}, \quad \mathbf{a}_2 = \begin{pmatrix} a_2 \cos\gamma \\ a_2 \sin\gamma \end{pmatrix},$$

then the basis vectors of the reciprocal space lattice are given by

$$\mathbf{b}_1 = 2\pi \frac{\mathbf{a}_2 \times \hat{\mathbf{z}}}{(\mathbf{a}_2 \times \hat{\mathbf{z}}) \cdot \mathbf{a}_1} = \frac{2\pi}{a_1 a_2 \sin\gamma} \begin{pmatrix} a_2 \sin\gamma \\ -a_2 \cos\gamma \end{pmatrix},$$

$$\mathbf{b}_2 = 2\pi \frac{\hat{\mathbf{z}} \times \mathbf{a}_1}{(\hat{\mathbf{z}} \times \mathbf{a}_1) \cdot \mathbf{a}_2} = \frac{2\pi}{a_1 a_2 \sin\gamma} \begin{pmatrix} 0 \\ a_1 \end{pmatrix}.$$

Only the lowest order diffraction peaks could be observed; however, we will demonstrate that all of the observed positional order can be explained by assuming local triangular packing corresponding to a rectangular Bravais lattice with a two molecule basis. This orthorhombic lattice satisfies the condition that $a_2 \cos\gamma = a_1/2$. This means that 4 of the six nearest-neighbor bonds have length a_2. As a result, reciprocal lattice vectors of magnitude b_1 have a degeneracy of 4 and those of magnitude b_2 have a degeneracy of 2.

Although fluctuations make true long-range crystalline order impossible in two dimensions,[59] quasi-long-range order, which is characterized by algebraic correlations, gives rise to a scattering intensity distribution in reciprocal space for which the distribution around the smallest wave vectors is only subtly different than that of a true two-dimensional crystal and it is convenient to discuss GID from a LM as though the system had true two-dimensional long-range order.

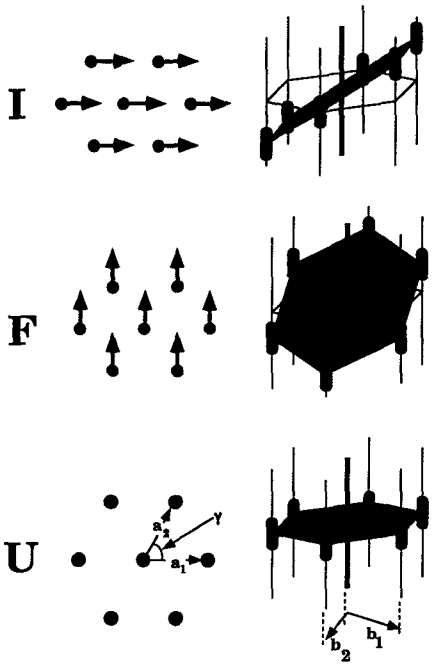

FIG. 6. Representation of the expected diffraction patterns for the three types of two-dimensional phases seen in this study. The projection of the molecular tilt onto the plane of the surface is shown on the left and the corresponding reciprocal space lattice on the right. The real and reciprocal space lattice parameters are shown. The shaded hexagon represents the plane of the long axes of the oblate ellipsoid described in the text and the darkened cylinders indicate the intersection of the oblate ellipsoid with the rods of scattering in reciprocal space.

For a two-dimensional lattice of point objects, the theoretical scattering intensity has infinite extent in the third (Q_z) dimension, e.g., the structure factor of the lattice is a set of rods distributed on the two-dimensional reciprocal lattice. The effect of the finite molecular size on the scattering distribution from an actual monolayer is to multiply the uniform intensity along the rod by the molecular form factor which, in the kinematic approximation, is the square of the magnitude of the Fourier transform of the electron density of the individual molecule. Some features of the scattering distribution from such monolayers are relatively independent of the details of the electron distribution of an individual molecule. For example, if the molecule is modeled as either a uniform rod of finite length, or a prolate ellipsoid, then the Fourier transform will be either a flat disk or an oblate ellipsoid. We will avoid questions of oscillations in the Fourier transform by assuming that the electron density does not have a hard edge, but dies off gradually, e.g., as a Gaussian. This oblate ellipsoid multiplies the array of rods. If the molecules in the film are oriented with their long axis normal to the x-y plane, then the ellipsoid will lie in the $Q_x - Q_y$ plane in reciprocal space. The maximum intensity along each rod is predicted to be where the center of the ellipsoid intersects the rod, in this case at $Q_z = 0$ (phase U in Fig. 6). However, if the molecules are tilted away from the surface normal, then the ellipsoid in reciprocal space will cut through the rods at an angle, moving the maximum intensity along the rods away from $Q_z = 0$ in some cases.

In order to determine where the maximum intensity will be for a particular rod, we must know not only the tilt angle of the molecule from the surface normal, θ, but also the azimuthal direction of the tilt, ϕ, in relation to the surrounding lattice. In general the value of Q_z for which the intensity is maximum along the rod is given by

$$Q_z^{\max} = \mathbf{Q}_\perp \cdot \begin{pmatrix} \cos\phi \\ \sin\phi \end{pmatrix} \tan\theta, \tag{5}$$

where ϕ is angle between the projection of the molecular tilt and the x axis.

The only three phases observed in this study of C24 correspond to one untilted phase ($\theta = 0$), one tilted phase in which $\phi = 0$, corresponding to the molecules tilting towards their nearest neighbor, and another in which $\phi = \pi/2$, corresponding to the molecules tilting midway between neighbors. Figure 6 illustrates the location of the intensity maxima relative to the reciprocal lattice for the two tilted cases of interest. We will call the case in which $\phi = 0$ the I phase and one with $\phi = \pi/2$ the F phase in analogy to the smectic liquid crystal phases with the same in-plane structure.[60] We see that in the I phase two peaks remain at $Q_z = 0$ while two peaks move up to positive Q_z and two move to a negative value. In the F phase all peaks move away from $Q_z = 0$. Of the three at positive Q_z, two move to the same value of Q_z and the third moves to a value of Q_z that is twice as large. The situation is symmetrical at negative Q_z. This gives us distinct signatures of the three phases: untilted, I, and F.

The picture, in reciprocal space, for a two-dimensional powder can be constructed from the aforementioned patterns by simply rotating the entire reciprocal space around an axis perpendicular to the $Q_x - Q_y$ plane and passing through the origin. This converts all peaks into rings, and removes the distinction between Q_x and Q_y making it convenient to speak of $Q_\perp$.

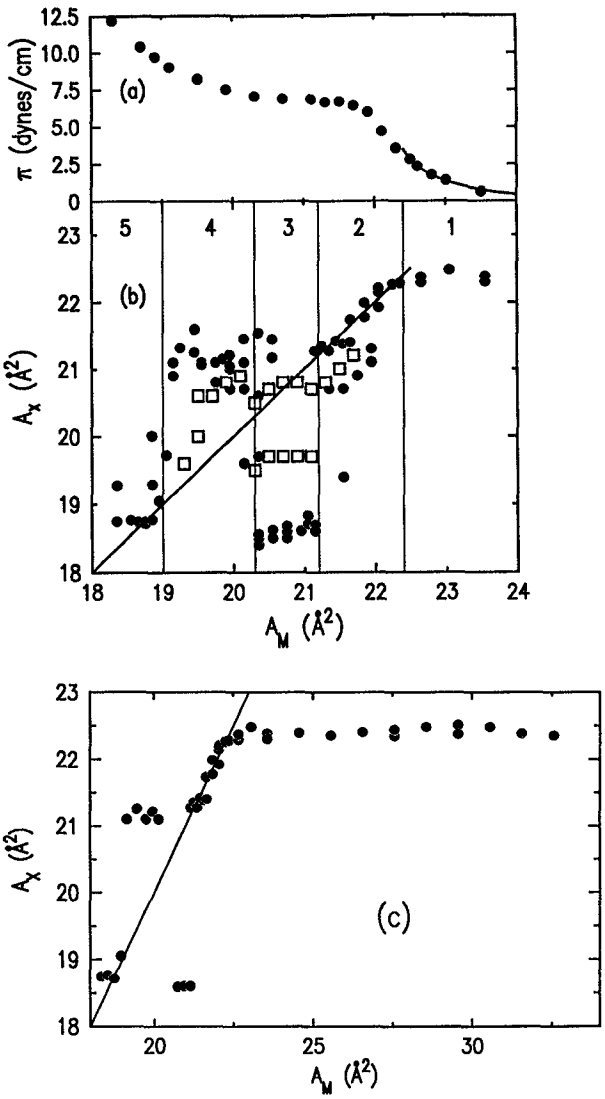

FIG. 7. (a) A typical isotherm for tetracosanoic acid at ~20.5 °C divided into numbered regions. (b) Unit cell area, A_x plotted vs deposited area per molecule A_M. The filled circles represent the results for a fully relaxed monolayer, while the the results represented by unfilled squares were taken on a monolayer that was not fully relaxed, as described in the text. The solid line is the result to be expected for a microscopically homogeneous monolayer. (c) The same axes as Fig. (b) displayed over a larger region.

VI. X-RAY RESULTS

Figure 7, summarizing the results of diffraction measurements on the monolayer phases of tetracosanoic acid at $T \cong 20.5$ °C, is divided into five regions with different physical properties. The isotherm in part (a) was taken simultaneously with the diffraction measurements for one of the monolayers. Part (b) illustrates the variation of A_x with A_M for 6 different monolayers, where A_x is the area/molecule calculated from the observed diffraction peaks and A_M is the area/molecule calculated from the amount of material deposited in the monolayer. To account for systematic errors (i.e., ± 0.5 Å), the values of A_M for different monolayers were shifted to ensure that their isotherms overlapped. The solid line, corresponding to $A_x = A_M$, shows what is expected for a homogeneous film in which the total area A_T is given by $A_T = NA_M$ and illustrates the result that in only two of the five regions indicated on the isotherm is the film believed to be homogeneous. The scatter of the equilibrium points is due primarily to the result of small temperature differences for these six different monolayers. Although there is some slight temperature dependence to the pressure and to the range of area over which a particular phase persists, the sequence of phases is unchanged over the measured temperature range of 20–22 °C whenever the waiting time between incremental changes in area was sufficiently long to allow the surface pressure π and the diffraction pattern to stabilize. In certain parts of the phase diagram, notably region 3, stable diffraction patterns were only observed during the final stages of pressure relaxation. This sometimes required an order of magnitude longer than the time for the surface pressure to decay to $1/e$ of its initial value following incremental compression. Very different results were obtained if the surface pressure was not allowed to stabilize completely.

In principle, the functional form and width of the peaks give information about the type and extent of correlations that exist in real space. In practice, however, distinguishing an algebraic line shape from either a Lorentzian or a Gaussian shape relies on subtle features that are not supported by

the existing data (in particular, the statistics). As a result, since the data do not allow us to distinguish between the two line shapes, it was convenient to fit the peaks to a Gaussian line shape for which a linear background is added as an approximation to the bulk scattering. Peak widths mentioned are Gaussian widths, and real-space correlation lengths are corrected for resolution effects and computed as $(\sigma\sqrt{2\ln 2})^{-1}$, where σ is the Gaussian width in reciprocal space.

A. Region 1

The only diffraction peaks seen throughout region 1 were those corresponding to the I phase. Within this region the equilibration times for the surface pressure π were short, ~ 30 s, and the peak positions were essentially independent of A_M. Representative lattice parameters are displayed in Table I and typical peaks in $Q_\perp$ are shown in Fig. 8. The plots on the left of the figure display the peaks at the value of Q_z where the peak intensity is greatest. The plots on the right show peak amplitude plotted vs Q_z for typical peaks. The solid dots represent the measurements and the solid lines represent the fits. Theoretically, the Q_z dependence of these peaks should yield information about the structure of the molecule in the surface normal direction. In practice, the statistics are too poor to allow detailed analysis. However, by modeling the molecule density as a simple square wave with thickness L_z we can fit the peaks in Q_z to the form

$$I(Q_z) \propto \left(\frac{\sin(Q_z L_z/2)}{Q_z L_z/2}\right)^2.$$

For all of the region 1 these fits give values of $L_z = 27 \pm 2$ Å. This degree of accuracy is not sufficient to distinguish between the values L_z for the different phases; however, it does agree with the thickness that was extracted from the specular reflectivity measurement for the low pressure portion of region 2 that will be discussed below. The area A_x computed from the positions of the diffraction peaks is less than the deposited average area per molecule (see Fig. 7). This implies that the film is not homogeneous, and that there are empty regions or regions of lower density on the surface. The peaks are resolution limited, implying that the ordered phase consists of large crystalline (or hexatic) domains coexisting with some dilute, noncrystalline phase, possibly an ideal gas of impurities. A lower bound for the size of correlated regions, based on the resolution limit, is 240 Å.

In this region, the film appeared to be a coarse powder

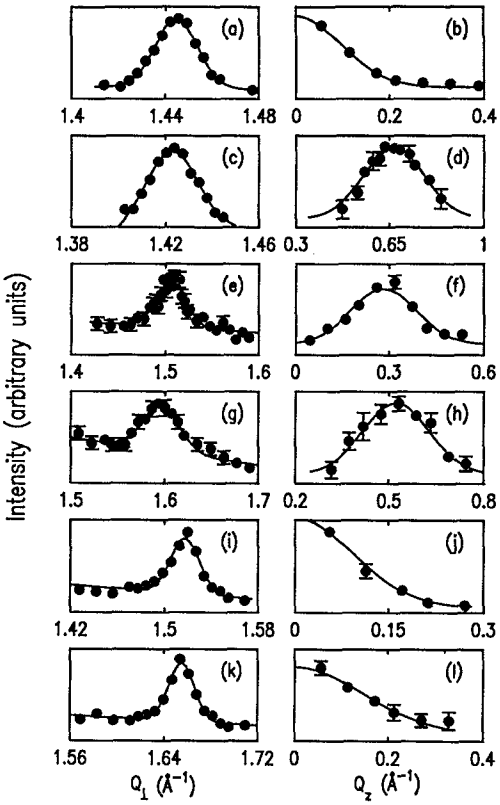

FIG. 8. Typical peaks for all three phases are shown. The plots on the left are scans in $Q_\perp$ at the value of Q_z for which the intensity is greatest. The plots on the right show the peak intensity of the $Q_\perp$ scan as a function of Q_z. (a),(b) and (c),(d) I phase, (e),(f) and (g),(h) F phase, and (i),(j) and (k),(l) the untilted or U phase.

since there were large fluctuations in intensity between the peaks seen at positive and negative Ψ, and also between different films. We attempted to examine this in more detail by rotating the sample; however, it was not possible to rotate the trough without also causing slight tilts that led to flow in the liquid subphase. Changes in the monolayer accompanying even small rotations of the trough were not reversible. Nevertheless, we can estimate the size of the crystalline islands from the stochastic fluctuations of the peak intensity. Although we sometimes saw fluctuations at the level of 50% in intensity we will take a conservative value of 10%. Assuming Poisson statistics, this means the x-ray beam sampled at most 100 correlated regions. To calculate the mean

TABLE I. Representative lattice parameters of the three phases. The parameters Q_{11} and Q_{21} are identical to the reciprocal lattice vectors b_1 and b_2 discussed earlier.

Phase	Q_{11}	Q_{1z}	Q_{21}	Q_{2z}	a_1	a_2	θ	a_1^{chain}	a_2^{chain}
		(Å^{-1})			(Å)		(deg)	(Å)	
I	1.420	0.79	1.445	0	5.14	5.05	33	4.30	4.86
U	1.517	0	1.655	0	4.94	4.53	0	4.94	4.53
F	1.50	0.24	1.60	0.50	4.92	4.64	15	4.92	4.52
F	1.494	0.28	1.578	0.54	4.95	4.689	19	4.95	4.50
F	1.493	0.33	1.539	0.66	4.91	4.764	22.6	4.91	4.49
	± 0.005	± 0.05	± 0.005	± 0.05	± 0.02	± 0.02	± 2	± 0.02	± 0.02

number of ordered domains consider that the angular spread of the incident beam was $\Delta\Phi \approx 0.12°$. Assuming that the orientations of the ordered domains were distributed isotropically within the plane of the surface, and considering that for each I domain there are two equivalent peaks at $Q_z = 0$, the total number of regions in the illuminated area was larger than the 100 correlated regions that were observed by a factor of $(1/2)(360°/0.12°)$, corresponding to 2×10^5 domains. Since A_x is not very much smaller than A_M, for an illuminated area of ~ 200 mm^2 the dimension of an ordered domain is of the order of $[200\ \text{mm}^2/(2\times 10^5)]^{1/2} = 30\ \mu$m. This is similar to domain sizes measured with fluorescence microscopy in monolayers of lipids and other fatty acids.[61-63]

B. Region 2

When A_M decreases past approximately 23 Å^2/molecule the equilibration time of the monolayer rises dramatically from a few minutes to several hours. At the same area the pressure starts to deviate from the ideal gas behavior and over the next ~ 2 Å^2/molecule π rises sharply. As shown in Figs. 9 and 10 this is accompanied by an equally dramatic change in the dependence of the peak positions, tilt angle, and peak widths on deposited area/molecule, A_M.

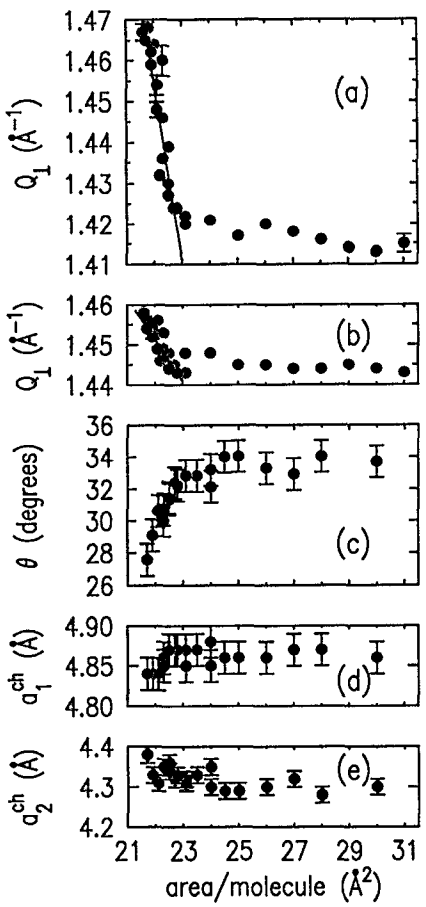

FIG. 9. The top two plots show the positions of the peaks in the I phase as a function of area A; (a) the peak at nonzero Q_z, (b) the peak at $Q_z = 0$. (c) The value of θ as calculated from Eq. (5). (d) and (e) The values of the chain-packing lattice parameters as described in the text. Notice that they are unchanged throughout the phase.

Notice that in region 1, both peak positions are unchanged within the error bars. However, as the film enters region 2 the peaks begin to shift position linearly with the deposited area. The shift in $Q_\perp$ for the peak at positive Q_z is larger than that for the peak at $Q_z = 0$. The slope of the linear region for the high Q_z peak is -0.043 ± 0.003 Å^{-3}, while for the $Q_z = 0$ peak the slope is -0.010 ± 0.001 Å^{-3}. This indicates that the lattice is compressed primarily, though not entirely, along the a_1 axis (the projected tilt direction for the I phase).

This compression is accompanied by a change in the position of maximum intensity in Q_z for the peak at $Q_z \neq 0$. The position systematically decreases, implying a reduction of the tilt angle θ [see Fig. 9(c)]. The value of θ has been calculated by simply inverting Eq. (5) and substituting $\phi = 0$ for the I phase. The change in θ can be simply related to the compression if we consider the packing of the hydrocarbon chains. In Fig. 9 we illustrate the distances $a_{1,2}^{ch}$ between adjacent alkane chains in the plane that is normal to the chain axis. The chain packing distances for the I phase are given by

$$a_1^{ch} = a_1 \cos\theta,$$

$$a_2^{ch} = [(a_2 \cos\gamma \cos\theta)^2 + (a_2 \sin\gamma)^2]^{1/2}.$$

These adjusted lattice parameters are constant throughout regions 1 and 2 suggesting that the lattice parameters are determined by the packing constraints of the hydrocarbon chains. In a manner similar to bulk hydrocarbon chains, the closest packing occurs when an "H atom from one molecule enters the depression between three H atoms in an adjacent molecule".[64,65] Using this rule, only certain tilt angles are permitted for *all-trans* chains. For a monolayer of such chains with orthorhombic symmetry (as is appropriate here) Kitaigorodskii has tabulated these tilt angles as 34.5, 31.5, 27, 19, and 0 deg.[64] This is not to imply that other physical considerations may not determine the actual structure or tilt angle, for example, bulk paraffins often exhibit rotator phases in which the molecules have partial or complete freedom to rotate about the chain axis thus overcoming

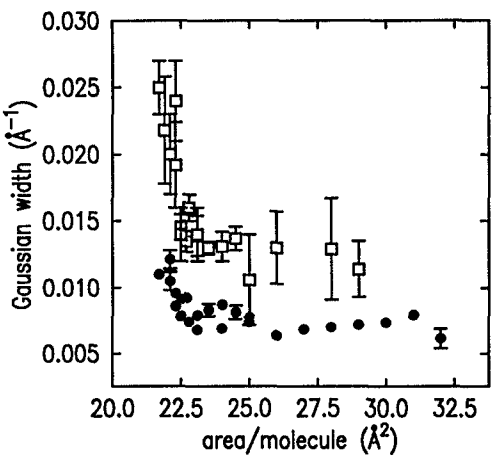

FIG. 10. Gaussian widths, σ_{Gaussian}, of peaks in the I phase [i.e., half-widths at half-maxima are given by $\sigma_{\text{Gaussian}}(2\ln 2)^{1/2}$]. The open squares show the widths of the peak at nonzero Q_z, the filled circles the peak at $Q_z = 0$.

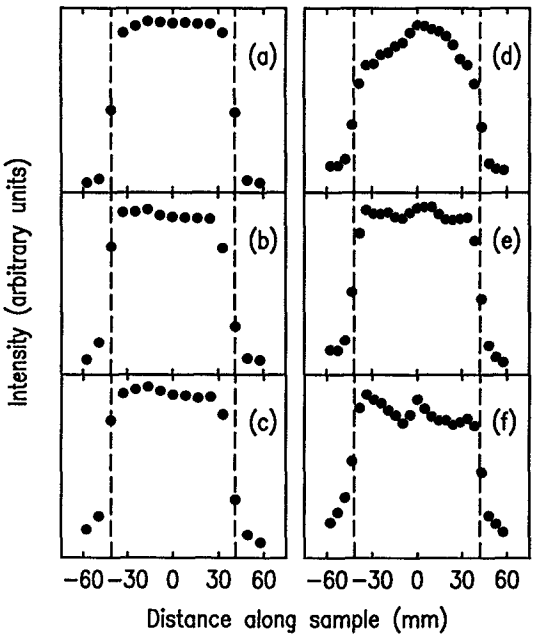

FIG. 11. Specular reflectivity as the beam is scanned across the sample surface. The plots marked (a), (b), and (c) were taken at incident angles of 1.0°, 2.1°, and 2.8°, respectively, and show typical scans for regions 2 or 5 where the film is uniform. The scans marked (d), (e), and (f) were taken at incident angles of 2.6°, 3.0°, and 3.5°, respectively, in region 3, but are also typical for region 4. The scans are reproducible and not due to surface curvature, indicating an inhomogeneous film in these regions. The lines indicate the edges of the sample.

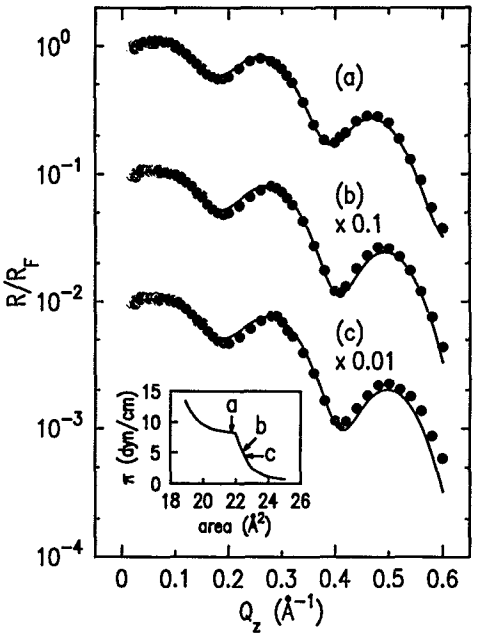

FIG. 12. (a) Reflectivity at three different areas within region 2. The filled circles are x-ray data and the lines represent fits to Eq. (4). (b) The inset shows where on the isotherm the three sets of data were taken, (a) 8.2 dyn/cm, (b) 5.2 dyn/cm, and (c) 4.5 dyn/cm.

the constraint of nesting the H atoms. Alternatively, Cai and Rice have used a density functional theory to show that monolayers of rigid cylinders (no effects due to nesting) will often prefer a tilted rather than an untilted configuration and that there is a free energy minimum for a tilt angle of approximately 30°.[66,67] In either case, as the area/molecule is externally varied under conditions that force the tilt angle to deviate from an energetically optimum value, it is likely that the accompanying rise in free energy of the monolayer will destabilize the I structure.

Furthermore, we might expect the correlations of the two-dimensional order to suffer because of this additional "strain" free energy. In fact, as the monolayer is progressively compressed into region 2, the widths of the peaks broaden significantly (see Fig. 10) indicating a reduction in the in-plane correlations from $\geqslant$240 Å at large areas, to a value of 190 Å. Note that for $A > 23$ Å^2 both peaks representing the I phase are resolution limited, but the $Q_z > 0$ peak widths are larger than the $Q_z = 0$ widths due to the change in the spectrometer resolution as a function of Q_z. In this region the plot of the unit cell area (A_x) vs deposited average area per molecule (A_M) [Fig. 7(b)] is linear with a slope close to 1, implying that the monolayer is homogeneous.

Finally, Figs. 11(a)–11(c) illustrate specular reflectivity for three different incident angles α as a function of the position of a narrow x-ray beam ($\sim$3 mm footprint) along the length of the sample. The fact that the reflectivity is essentially independent of position for approximately 90 mm, corresponding to approximately the length of the subsurface quartz flat, supports the contention that the LM is homogeneous. Figure 12 shows reflectivity data at three different surface pressures within region 2. The solid lines through the data represent fits to the model described by Eq. (4). The values and uncertainties in the model parameters for the data sets are given in Table II. We can notice some interesting results. The thickness of the tail region, which is closely related to the parameter L, increases monotonically with π. Assuming that the chains are rigid, this is just what is expected from the previous analysis of the tilt angle θ extracted from the diffraction data. The values of θ in Table II are taken from the analysis of the diffraction data and the molecular length is simply calculated as $L/\cos\theta$. If we make the simplifying assumption that the length of the C–O bonds in the head group are the same as all of the C–C bonds then the repeat distance along the alkane chain is given by $2\times(32/25) = 2.56$ Å which is equal to typical published values.[68]

The result for the width of the tail/vapor interface σ_1 is in good agreement with the value expected for a roughness due to thermally excited capillary waves at such an interface. The value expected for a pure water surface is 2.69 Å (Ref. 25) with the particular spectrometer configuration used. This value should scale, however, as $1/\sqrt{\gamma}$, where γ is the surface tension. Therefore the value of σ_1 expected from capillary wave considerations should range from 2.78 Å at $\pi = 4.5$ dyn/cm to 2.86 Å at $\pi = 8.2$ dyn/cm. The measured value is within 0.2 Å in all cases, although the trend towards decreasing roughness with increasing surface pressure is the opposite of what one would expect if σ_1 was due to only thermal capillary waves. This could be due to a number of different effects such as if, for example, the increase in sur-

TABLE II. Fitted parameters for reflectivity data. The tilt angle θ is taken from the diffraction analysis and the molecular length, L_{mol} is simply calculated from $L_{mol} = L/\cos\theta$.

π (dyn/cm)	A_1	σ_1	L (Å)	A_2	σ_2 (Å)	θ (deg)	L_{mol} (Å)
4.5	0.986 ± 0.005	2.95 ± 0.026	27.01 ± 0.12	0.924 ± 0.051	3.16 ± 0.13	31.5 ± 2	31.7 ± 0.8
5.2	0.986 ± 0.005	2.84 ± 0.024	27.34 ± 0.11	0.946 ± 0.048	3.1 ± 0.12	30.0 ± 2	31.5 ± 0.6
8.2	$0.995 \pm .004$	2.78 ± 0.019	28.64 ± 0.10	0.88 ± 0.04	3.38 ± 0.11	27.0 ± 2	32.1 ± 0.7

face pressure caused a reduction in the number of gauche bonds in the alkane chains, or if the increase in surface density imparted some shear elasticity to the monolayer.

The electron density in the tail region is very close to that of water, only 1%–2% less, and comparable to values measured for crystalline alkanes.[68] From the values for the parameter A_2 and the areas A_x one can extract a value for the excess number of electrons in the head group region, i.e., the number of electrons in the head group that contribute to an electron density larger than that of the surrounding tail group and water. For the three data sets described in Table II there are an average of 6.6 ± 0.5 electrons per head group which corresponds well with the expected 7 electrons per head group.[69]

To summarize, we interpret region 2 as a homogeneous crystalline powder in which the molecules systematically tilt towards the surface normal and move closer together as the density is reduced.[66] The total compression of the lattice is about 3% of the lattice constant and we believe that the local stresses associated with this strain is the origin of an instability that gives rise to the transition from region 2 to region 3.

C. Region 3

At areas A_M, slightly smaller that that of the "knee" in the isotherm but still in Region 2 (approximately 21.5 Å), diffraction peaks associated with an F phase were sometimes observed in coexistence with the I phase peaks. The Q_z dependence of the peaks in the F phase are shown in Figs. 8(f) and 8(h). Near to the boundary between regions 2 and 3 the intensities of the diffraction peaks of both the I and F phases were often small and sometimes only the peak at smaller Q_1 was visible for each phase. At other times, all four peaks could be seen and, for a small range of density at the boundary between regions 2 and 3, when observed the peaks were stable over periods of at least 6 h. The coexistence was seen over a very narrow region in area/molecule, usually $\leqslant 0.2$ Å^2/molecule. As will be discussed, F phases also appear occasionally at the boundaries between regions 3, 4, and 5.

Upon further compression, following waiting periods that were often in excess of 2–3 h, the monolayer relaxed into the stable, and what we believe to be the equilibrium, untilted (U) phase. This relaxation proceeded via untilting of molecules that were originally in the F phase. For several monolayers, *at a fixed area*, we were able to follow as a function of time the movement of the diffraction peaks from those for the F phase to those for the U phase. In this sense the F phase is the precursor to the U phase and, as mentioned, is present whenever the U phase is appearing or disappearing. In further support of this mechanism, Table I shows that the F phase interchain lattice constants, $a_{1,2}^{ch}$, in the plane normal to the chain axis, are independent of tilt angle θ and equal to the corresponding values in the U phase, suggesting that chain packing is identical in the two phases. Since a_1 is perpendicular to the direction of tilt, a_1^{ch} is simply equal to a_1. The distance a_2^{ch} for the F phase is given by the expression

$$a_2^{ch} = [(a_2 \sin\gamma \cos\theta)^2 + (a_2 \cos\gamma)^2]^{1/2}.$$

Relaxation into the U phase can take as long as 6 h. During this relaxation, π relaxed to very close to its final value after 30 min. However, within the next few hours it was usually observed to relax by an additional $\Delta\pi \approx 0.1$ dyn/cm. Occasionally, even after this relaxation an F phase would remain in coexistence with a U phase. In that circumstance, an additional incremental compression was required for the F phase to disappear, leaving only peaks due to the U phase. If the waiting period between incremental compressions was shorter than that required for full relaxation, or if the monolayer was continuously compressed from a low density, the peaks corresponding to the untilted phase were not seen at all and the entire region 3 looked like a coexistence of I and F phases. This is demonstrated by the difference between the filled circles (equilibrium) and the unfilled squares (nonequilibrium) in Fig. 7.

Once completely in the untilted phase the film was very stable and the lattice constants remain unchanged as A_M varied throughout the entire region. Representative lattice parameters for this phase are listed in Table I. The Q_z dependence of the peaks in the untilted phase are shown in Figs. 8(j) and 8(l). The unit cell area is small, in fact it corresponds well to that of crystalline bulk hydrocarbon lattices with untilted chains.[68] In this region the film cannot be homogeneous since the unit cell area A_x is smaller than the deposited area per molecule A_M. It follows that the observed domains of untilted phase crystallites must coexist with areas of a less dense phase that is not observed by diffraction. Since this less dense phase has no diffraction signature, it is probably amorphous.

Additional diffuse scattering is to be expected from the amorphous fractions of the surface monolayer; however, in view of the relatively large amount of diffuse scattering from the water below the monolayer it is difficult to detect and none was observed. We have measured diffuse scattering from the monolayer in excess of that measured from the pure water surface, but this was not studied systematically.

Further evidence to support the idea of an inhomogen-

eous film was provided by comparing the x-ray reflectivity from different positions on the surface of the trough. As can be seen in Figs. 11(d)–11(f). in contrast to similar data from region 2, the reflected intensity varies by as much as 30% when the small x-ray beam (~3 mm footprint) moves across the sample. Because the angular spread of the reflected beam was identical to that of the direct beam, and the position of the reflected beam was independent of position on the surface we do not believe this variation was an artifact due to, for example, sample curvature.

As we suggested previously, compression of the monolayer area in the I phase has the effect of forcing the molecules to occupy an area that is smaller than the one favored for optimum interchain packing. It appears as though the interplay between the F and U phases is a further manifestation of the manner in which the monolayer responds to this strain. First, when the F and U phases are seen together, the F phase can have a range of tilt angles from 14°–23°. Second, the F phase peaks are broadened considerably in both Q_z and $Q_\perp$, suggesting that in the same sample there are a range of different tilt angles as well as in-plane correlation lengths of only 140 Å. When the monolayer relaxes into the U phase the diffraction peaks are resolution limited with a lower limit to the in-plane correlation length of 240 Å. These observations imply that the F phase is a very strained phase which relaxes to the U phase.

We do not believe that the formation of the F phase is due to anisotropic compression of the monolayer by the trough. If this were the case, then we would expect that part of the film would not be converted to the F phase and would remain in the I phase throughout region 3, in contradiction with our observations.

To summarize, we interpret the relaxed version of region 3 as coexistence between positionally ordered domains of the high density untilted U phase and a lower density disordered phase. Although it appears as though this coexistence is stable over periods in excess of 10–15 h, its microscopic origin is a matter of speculation.

D. Region 4

The boundary between regions 3 and 4, at approximately 20 Å^2/molecule is indicated by the reentrant appearance of the I phase following an incremental compression. Although the diffraction peaks associated with the I phase are clearly the dominant features, they occasionally appear in coexistence with those of the F phase. This is reminiscent of the coexistence observed on the boundary between regions 2 and 3. The lattice constants of the reentrant I are the same as at the end of region 2, i.e., the most compressed I phase. This very surprising phase sequence was repeatable and reversible (Fig. 13), i.e., upon expansion of the film the reentrant I phase disappeared and the untilted phase reappeared. In addition, although there was a small hysteresis in the area A_M ($\Delta A_M \leqslant 0.5$ Å^2), as a function of surface pressure the $U \leftrightarrow I$ transition is quantitatively reversible (see Fig. 13). We suspect that the hysteresis in area is an experimental artifact due to pinning of the water meniscus along the edges of the trough or barrier. This reversibility in surface pressure lends credence to the argument that this is an equilibrium phase

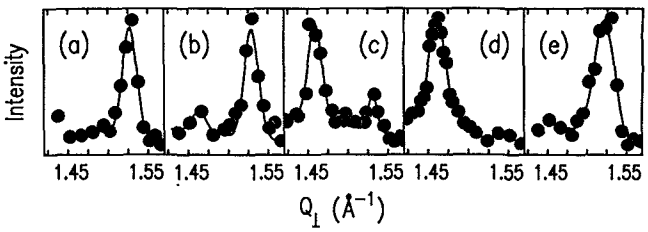

FIG. 13. A sequence showing only the lowest $Q_\perp$ peaks as the film is compressed from the untilted U phase to the I phase and then expanded. The sequence goes left to right. Panel (a) shows the untilted phase, while the next two (b) and (c) show coexistence between the untilted and reentrant I. Panel (d) shows a pure re-entrant I phase. Panels (a)–(d) were on compression. After re-expanding the film the untilted phase came back as shown in panel (e). The surface pressures π for the panels are: (a) 5.90, (b) 6.12, (c) 6.15, (d) 6.33, and (e) 6.06 dyn/cm.

sequence and not an artifact due to, e.g., lost material.

The lattice constants throughout region 4 are constant, but since the unit cell area is larger than the deposited area/molecule the film in this region must still be inhomogeneous. This time, however, the noncrystalline coexisting phase must be more dense than the diffracting I phase. X-ray reflectivity across the sample was again nonuniform in this region.

E. Region 5

The end of region 4, and the start of region 5 at approximately 19 Å^2/molecule, is characterized by the reappearance of the untilted U phase. The transition region is similar to the transitions between regions 2 and 3, and between regions 3 and 4, in that the F phase is nearly always seen in coexistence. Full relaxation into the untilted phase often requires several hours. This region differs from region 3 in the fact that the unit cell area A_x is essentially identical to the deposited area per molecule A_M as is expected for a homogeneous film. Although not conclusive, all of the observations we have made, including the fact that the x-ray specular reflectivity is constant across the film surface, are consistent with the conclusion that the monolayer in this region, like that of region 2, is a homogeneous film.

VII. DISCUSSION

Regions 1 and 2 contain large domains with well developed positional order which could be either crystalline or hexatic. In region 1 these ordered domains coexist with a dilute gas phase, which, in our case, probably contains a finite concentration of impurities that are insoluble in both the two-dimensional ordered phase and the liquid subphase. The impurities would then be responsible for the fact that $d\pi/dA \neq 0$ during coexistence. Alternatively, it is conceivable that the finite $d\pi/dA$ in region 1 results from electrostatic, or other, repulsion between islands[70] whose maximum dimension is determined by internal frustrations in the molecular packing. More experimental work is needed to distinguish between these possibilities. When the domains are brought together, which is somewhere near the boundary

between regions 1 and 2, further incremental compression forces the domains against one another and we believe that the increased times that are required for π to stabilize are due to the relaxation of either grain boundaries or other internal structural defects. Eventually, when the area/molecule A_M on the surface becomes equal to the unit cell area A_x the excess free area associated with the grain boundaries is reduced to a negligible fraction and further compression decreases A_x.

The diffraction data in the low density region 1 is consistent with a structure in which the alkane chains are packed with a tilt angle of approximately 32°–34°. We assume that this is the configuration favored by the microscopic interactions of the alkane chains under the relatively weak constraints that exist at low density. After the free space between the domains becomes negligible there is a small range of incremental compression (region 2) during which the surface pressure increases, the azimuthal tilt direction of the molecules remains unchanged and the tilt angle of the tail groups decreases. This happens in such a way that the parameters that describe the packing of the alkane chains, in a plane that is normal to their long axis, remain constant. If we assume that the ends of the chains are fixed at the water interface, the geometry of changing the chain tilt angle necessitates some relative sliding of adjacent chains over one another. The total "slide" along the chain length as θ changes from 34°, in the low density phase, to 27°, when the phase eventually collapses at the boundary between regions 2 and 3 is of the order of 0.5 Å. We hypothesize that the strain energy associated with this displacement must be enough to raise the chemical potential of the homogeneous I phase enough so that some sort of inhomogeneous phase is more stable.

Although we can observe only the ordered fraction of the monolayer in regions 3 and 4, it is clear that both regions are inhomogeneous, and in both cases, only one of the two existing phases is ordered enough to diffract x-rays. This part of the isotherm has typically been considered as a coexistence region between two phases and, although it is bracketed by regions 2 and 5, which we believe to be homogeneous I and U phases, respectively, it is not clear that it should be regarded as a region of simple coexistence between two phases which are in thermodynamic equilibrium. In fact, according to the usual lever rule of coexistence, the ordered phases that we observe by diffraction should be in the minority in the regions in which we see them. In addition, if this were a simple coexistence such as that observed by Barton *et al.* for monolayers of a partially fluorinated fatty acid ($C_{10}F_{21}CH_2COOH$) one would expect that the relative intensities of the diffraction peaks from the two types of phases would vary across the coexistence region in a continuous manner in accordance with the lever rule.[23] This is not what is observed, since in both regions 3 and 4 the intensities of the respective U and I phase peaks are essentially constant. One possibility is that in regions 3 and 4 there is some kind of coexistence, between a well ordered minority phase and a highly strained, and thus disordered, majority phase; the latter being so highly strained that its diffraction signal is unobservable. We suspect that this might be rationalized in terms of some kind of internal frustration that places a limit on the size of correlated domains; however, we have not formulated a satisfactory model.

There are several possible candidates for the source of the frustration. One possibility is a basic incommensurability between the optimum packing of the alkane chains and that of the molecular head groups at the water surface.[71–73] The mean free area per chain is a function of the tilt angle and, as we have seen, compression causes this to change from some optimum value at low densities and pressures. Safran and others have produced a quantitative argument in which frustration associated with the tilt degree of freedom leads to domains of finite size.[71–73] Also, we know that at low density the surface contains approximately 0.5% impurities and some fraction of these could be incorporated into the ordered parts of the film. These could be responsible for disturbances in the local packing and Nelson and co-workers have shown that the presence of quenched random impurities in a two-dimensional system can lead to reentrant behavior.[74,75] We believe that the level of impurities in our system is comparable to or better than that in other x-ray studies of Langmuir monolayers and, therefore, under the appropriate conditions of relaxation, effects similar to those we have demonstrated should appear in other systems.

In some respects the effects reported here in which increased surface pressure induces a phase transition from the crystalline I phase (region 2) to region 3, in which an unseen amorphous phase coexists with the U phase is similar to pressure induced amorphization that has recently been observed in three-dimensional systems. For example, following the seminal discovery that high pressures can cause the amorphization of crystalline H_2O ice[76] a number of investigators have observed pressure induced amorphization in crystalline silica.[77–79] Recent studies have shown this amorphization to be reversible.[80,81] Although this phenomenon has not previously been observed in Langmuir monolayers we are not aware of any earlier experiments which studied phase sequences in relaxed monolayers similar to those reported here. Obviously, more experimental studies are needed, both to investigate the equilibrium behavior in the plateau region of other molecular systems and to establish the underlying mechanism which stabilizes the phase sequence we have described.

ACKNOWLEDGMENTS

We acknowledge conversations with D. R. Nelson, G. M. Whitesides, C. A. Brown, S. A. Rice, and B. Lin. This work was supported by the National Science Foundation through Grants No. NSF-DMR-88-12855 and No. NSF-DMR-89-20490. Research carried out at the NSLS, Brookhaven National Laboratory, is supported by the Department of Energy, Material Sciences and Division of Chemical Sciences under Contract No. DE-AC02-76CH00016.

[1] G. L. Gaines, *Insoluble Monolayers at a Liquid Gas Interface* (Wiley, New York, 1966).

[2] W. Rabinovitch, R. F. Robertson, and S. G. Mason, Can. J. Chem. **38**, 1881 (1960).
[3] N. R. Pallas and B. A. Pethica, Langmuir **1**, 509 (1985).
[4] B. Lin, J. B. Peng, J. B. Ketterson, P. Dutta, B. N. Thomas, J. Buontempo, and S. A. Rice, J. Chem. Phys. **90**, 2393 (1989).
[5] M. L. Schlossman, D. K. Schwartz, P. S. Pershan, E. H. Kawamoto, G. J. Kellogg, and S. Lee, Phys. Rev. Lett. **66**, 1599 (1991).
[6] R. M. Kenn, C. Bohm, A. M. Bibo, I. R. Peterson, H. Möhwald, K. Kjaer, and J. AlsNielsen, J. Phys. Chem. **95**, 2092 (1991).
[7] S. W. Barton, B. N. Thomas, E. B. Flom, S. A. Rice, B. Lin, J. B. Peng, J. B. Ketterson, and P. Dutta, J. Chem. Phys. **89**, 2257 (1988).
[8] K. Kjaer, J. Als-Nielsen, C. A. Helm, P. Tippman-Krayer, and H. Möhwald, J. Phys. Chem. **93**, 3200 (1989).
[9] T. M. Bohanon, B. Lin, M. C. Shih, G. E. Ice, and P. Dutta, Phys. Rev. B **41**, 4846 (1990).
[10] B. Lin, M. C. Shih, T. M. Bohanon, G. E. Ice, and P. Dutta, Phys. Rev. Lett. **65**, 191 (1990).
[11] G. C. Nutting and W. D. Harkins, J. Am. Chem. Soc. **61**, 2040 (1939).
[12] D. K. Schwartz, The Phase Sequence of a Langmuir Monolayer as Determined by X-Ray Scattering, PhD thesis, Harvard University, 1991 (unpublished).
[13] Millipore Corp., Bedford, MA 01730.
[14] J. T. Baker Inc., 223 Red School Lane, Dept. LB-TR, Philipsburg, NJ 08865. No. 6900-05 Ultrex II Hydrochloric acid.
[15] Fluka Chemical Corp., 980 South Second St., Ronkonoma, NY 11779. No. 87110 Tetracosanoic Acid 99.5%.
[16] Sigma Chemical Co., P. O. Box 14508, St. Louis, MO 63178. No. L-6641 Lignoceric Acid 99%.
[17] J. T. Baker Inc., 223 Red School Lane, Dept. LB-TR, Philipsburg, NJ 08865. No. 9257-02 Resi-Analyzed Chloroform.
[18] Hamilton Co., P. O. Box 10030, Reno, NV 89520-0012. No. 1710RN syringe with No. 90607 12 in. needle.
[19] J. Als-Nielsen and P. S. Pershan, Nucl. Instrum. Methods **208**, 545 (1983).
[20] M. L. Schlossman and P. S. Pershan, in *Light Scattering off Liquid Surfaces*, edited by D. Langevin (Marcel Dekker, New York, 1991).
[21] E. Stenhagen, in *Determination of Organic Structures by Physical Methods*, edited by E. A. Braude and F. C. Nachod (Academic, New York, 1955).
[22] A. M. Bibo and I. R. Peterson, Adv. Mater. **2**, 309 (1990).
[23] S. W. Barton, A. Goudot, O. Boulassa, F. Rondelez, B. Lin, F. Novak, A. Acero, and S. A. Rice, J. Chem. Phys. (submitted).
[24] A. Braslau, P. S. Pershan, G. Swislow, B. M. Ocko, and J. Als-Nielsen, Phys. Rev. A **38**, 2457 (1988).
[25] D. K. Schwartz, M. L. Schlossman, E. H. Kawamoto, G. J. Kellogg, P. S. Pershan, and B. M. Ocko, Phys. Rev. A **41**, 5687 (1990).
[26] P. S. Pershan, A. Braslau, A. H. Weiss, and J. Als-Nielsen, Phys. Rev. A **35**, 4800 (1987).
[27] P. S. Pershan, Faraday Discuss. Chem. Soc. **89**, 231 (1990).
[28] S. A. Rice, Nature **316**, 108 (1985).
[29] J. Daillant, L. Bosio, B. Harzallah, and J. J. Benattar, J. Phys. 149 (1991).
[30] N. Dent, M. J. Grundy, R. M. Richardson, S. J. Roser, N. M. McKeown, and M. J. Cook, J. Chem. Phys. **85**, 1003 (1988).
[31] T. P. Russell, Mater. Sci. Rep. **5**, 171 (1990).
[32] G. S. Smith, C. R. Safinya, D. Roux, and N. A. Clark, Mol. Cryst. Liq. Cryst. **144**, 235 (1987).
[33] S. Gierlotka, P. Lambooy, and W. H. De Jeu, Europhys. Lett. **12**, 341 (1990).
[34] S. G. Wolf, M. Deutsch, E. M. Landau, M. Lahav, L. Leiserowitz, K. Kjaer, and J. Als-Nielsen, Science **242**, 1286 (1988).
[35] B. Park, F. Spaepen, J. M. Poate, D. C. Jacobson, and F. Priolo, J. Appl. Phys. **68**, 4556 (1990).
[36] L. G. Parratt, Phys. Rev. **95**, 359 (1954).
[37] M. Pomerantz, A. Segmullter, L. Netzer, and J. Sagiv, Thin Solid Films **132**, 153 (1985).
[38] R. A. Cowley and C. A. Lucas, Faraday Discuss. Chem. Soc. **89**, 181 (1990).
[39] S. M. Heald, H. Chen, and E. V. Barrera, Faraday Discuss. Chem. Soc. **89**, 21 (1990).
[40] R. van Silfhout, J. F. van der Veen, C. Norris, and J. E. MacDonald, Faraday Discuss. Chem. Soc. **89**, (1990).
[41] I. K. Robinson, E. Vlieg, and K. Kern, Faraday Discuss. Chem. Soc. **89**, 159 (1990).
[42] B. M. Ocko, J. Wang, A. Davenport, and H. Isaacs, Phys. Rev. Lett. **65**, 1466 (1990).
[43] B. Puis, J. M. Gay, J. W. M. Frenken, S. Gierlotka, J. F. van der Veen, J. E. MacDonald, A. A. Williams, N. Piggins, and J. Als-Nielsen, Surf. Sci. **222**, L845 (1989).
[44] W. Zhao, X. Zhao, M. H. Rafailovich, J. Sokolov, T. Mansfield, R. S. Stein, R. C. Composto, E. J. Kramer, R. A. L. Jones, M. Sansone, and M. Nelson, Physics B **173**, 43 (1991).
[45] S. K. Sinha, E. B. Sirota, S. Garoff, and H. B. Stanley, Phys. Rev. B **38**, 2457 (1988).
[46] M. K. Sanyal, S. K. Sinha, K. G. Huang, and B. M. Ocko, Phys. Rev. Lett. **66**, 628 (1991).
[47] Charles M. Nobler, Bull. Am. Phys. Soc. **36**, 491 (1991).
[48] M. Seul and M. J. Sammon, Phys. Rev. Lett. **64**, 1903 (1990).
[49] K. A. Suresh, J. Nittman, and F. Rondelez, Europhys. Lett. **6**, 437 (1988).
[50] D. Jacquemain, S. Grayer Wolf, F. Leveiller, M. Lahav, L. Leiserowitz, J. Deutsch, K. Kjaer, and J. Als-Nielsen, J. Phys. (Paris) Colloq. **50**, C7 (1989).
[51] J. Als-Nielsen, Top. Current Phys. **2**, (1986).
[52] D. Gibbs, B. M. Ocko, D. M. Zehner, and S. G. J. Mochrie, Phys. Rev. B. **38**, 7303 (1988).
[53] R. L. Headrick, I. K. Robinson, E. Vlieg, and L. C. Feldman, Phys. Rev. Lett. **63**, 1253 (1989).
[54] K. S. Liang, E. B. Sirota, K. L. D'Amico, and S. K. Sinha, Phys. Rev. Lett. **59**, 2447 (1987).
[55] E. MacDonald, Faraday Discuss. Chem. Soc. **89**, (1990).
[56] W. C. Marra, P. E. Eisenberger, and A. Y. Cho, J. Appl. Phys. **50**, 6927 (1979).
[57] S. G. J. Mochrie, D. M. Zehner, B. M. Ocko, and D. Gibbs, Phys. Rev. Lett. **64**, 2925 (1990).
[58] J. Robinson, M. Kerkar, and A. Forty, Faraday Discuss. Chem. Soc. **89**, 31 (1990).
[59] J. M. Kosterlitz and D. G. Thouless, J. Phys. C **6**, 1181 (1973).
[60] P. S. Pershan, *Structure of Liquid Crystal Phases* (World Scientific, Singapore, 1988), pp. 54–62.
[61] H. M. McConnell, L. K. Tamm, and R. M. Weis, Proc. Natl. Acad. Sci. **81**, 3249 (1984).
[62] M. Lösche, E. Sackmann, and H. Möhwald, Ber. Bunsenges. Phys. Chem. **87**, 848 (1983).
[63] Charles M. Knobler, in *Advances in Chemical Physics*, edited by S. A. Rice and I. Prigogine (Wiley, New York, 1990), p. 145.
[64] A. I. Kitaigorodskii, *Organic Chemical Crystallography* (Consultants Bureau, New York, 1961).
[65] D. A. Outka, J. Stohr, J. P. Rabe, J. D. Swalen, and H. H. Rotermund, Phys. Rev. Lett. **59**, 1321 (1987).
[66] Z-H. Cai and S. A. Rice, Faraday Discuss. Chem. Soc. **89**, 211 (1990).
[67] Zhong hou Cai and Stuart A. Rice, J. Chem. Phys. (submitted).
[68] B. Ewen, G. R. Strobl, and D. Richter, Faraday Discuss. Chem. Soc. **68**, 19 (1980).
[69] M. L. Schlossman, D. K. Schwartz, E. H. Kawamoto, G. J. Kellogg, P. S. Pershan, B. M. Ocko, M. W. Kim, and T. C. Chung, in *Materials Research Society Proceedings—Macromolecular Liquids*, edited by C. R. Safinya, S. A. Safran, and P. A. Pincus (North-Holland, New York, 1989), p. 351.
[70] David Andelman, Francoise Brochard, and Jean-Francois Joanny, J. Chem. Phys. **86**, 3673 (1987).
[71] S. Safran, M. O. Robbins, and S. Garoff, Phys. Rev. A **33**, 2186 (1986).
[72] J. M. Carlson and J. P. Sethna, Phys. Rev. A **36**, 3359 (1987).
[73] J. F. Sadoc and J. Charvolin, J. Phys. (Paris) **47**, 683 (1986).
[74] D. R. Nelson, Phys. Rev. B **27**, 2902 (1983).
[75] M. Rubinstein, B. Shraiman, and D. R. Nelson, Phys. Rev. B **27**, 1800 (1983).
[76] O. Mishima, L. D. Calvert, and E. Whalley, Nature **310**, 393 (1984).
[77] R. J. Hemley, A. P. Jephcoat, H. K. Mao, L. C. Ming, and M. H. Manghani, Nature **334**, 52 (1988).
[78] Y. Tsuchida and T. Yagi, Nature **347**, 267 (1990).
[79] Q. Williams and R. Jeanloz, Science **239**, 902 (1988).
[80] M. B. Kruger and R. Jeanloz, Science **249**, 647 (1990).
[81] C. Meade and R. Jeanloz, Geophys. Res. Lett. **1157**, 17 (1990).